CrossMark
click for updates

Excellent cryogenic magnetocaloric properties in heavy rare-earth based HRENiGa$_2$ (HRE = Dy, Ho, or Er) compounds

Dan Guo[1,2,3], Luis M. Moreno-Ramírez[2], Jia-Yan Law[2*], Yikun Zhang[1,3*] and Victorino Franco[2]

ABSTRACT RENiX$_2$ compounds, where RE = rare-earth element and X = *p*-block element, have been highly regarded for cryogenic magnetocaloric applications. Depending on the elements, they can crystallize in CeNiSi$_2$-type, NdNiGa$_2$-type, or MgCuAl$_2$-type crystal structures, showing different types of magnetic ordering and thus affect their magnetic properties. Regarding the magnetocaloric effect, MgCuAl$_2$-type aluminides show larger values than those of the CeNiSi$_2$-type silicides and the NdNiGa$_2$-type gallides due to the favored ferromagnetic ground state. However, RENiGa$_2$ gallides can crystallize in either NdNiGa$_2$- or MgCuAl$_2$-type structures depending on the RE element. In this work, we select heavy RE (HRE) elements for exploring the microstructure, magnetic ordering and magnetocaloric performance of HRENiGa$_2$ (HRE = Dy, Ho or Er) gallides. They all crystallize in the desired MgCuAl$_2$-type crystal structure which undergoes a second-order transition from ferro- to para-magnetic state with increasing temperature. The maximum isothermal entropy change ($|\Delta S_{iso}^{max}|$) values are 6.2, 10.4, and 11.4 J kg^{-1} K^{-1} (0–5 T) for DyNiGa$_2$, HoNiGa$_2$, and ErNiGa$_2$, respectively, which are comparable to many recently reported cryogenic magnetocaloric materials. Particularly, the excellent magnetocaloric properties of HoNiGa$_2$ and ErNiGa$_2$ compounds, including their composite, fall in the temperature range that enables them for the in-demand hydrogen liquefaction systems.

Keywords: rare-earth-nickel-gallides, magnetocaloric effect, magnetic phase transitions

INTRODUCTION

Cooling technology has become an indispensable application in our modern society, in which the choice of optimal refrigeration technologies needs to be driven by environmental compatibility and energy efficiency. Regarding these aspects, the magnetic refrigeration (MR) technology based on the magnetocaloric effect (MCE), is expected to become a highly competitive cooling method due to its high-energy efficiency and the absence of hazardous and ozone-depleting gases in comparison to the conventional vapor-compression refrigeration [1–6]. The MCE is an inherent magneto-thermodynamic phenomenon that

occurs in magnetic materials upon changing the external magnetic field, which is significant at temperatures close to the thermomagnetic phase transitions. It is characterized by an isothermal magnetic entropy change (ΔS_{iso}) and an adiabatic temperature change (ΔT_{ad}). By using a large variety of magnetic materials and different thermodynamic cycles, MR can operate in a very wide temperature range (from extremely low temperatures up to room temperature) [7–17]. In recent years, low-temperature MR has received extensive attention due to its important applications, such as industrial gas liquefaction and storage, cryogenic space technology, and laboratory cryogenic basic research [18–25]. Liquid H$_2$ is a clean fuel that is widely used in the aerospace field and is expected to extend its use towards conventional applications. Moreover, for H$_2$ storage and transportation, the liquid state is more advantageous than the gaseous H$_2$. Regarding the liquefaction processes, the efficiency of magnetic systems could reach 60% of the theoretical Carnot cycle, which is 50% higher than the actual ones of gas compression systems [26].

For these reasons, exploring MCE materials with excellent performance in the low-temperature range is of great interest. Specifically, it has been reported that several heavy rare-earth (HRE)-transition metal (TM) intermetallic compounds can be considered potential candidates for cryogenic MR materials for H$_2$ liquefaction [27–33]. This is due to the large total orbital quantum numbers (*J*) of HRE elements, which lead to large magnetic moments that are beneficial to the magnetocaloric properties. Recently, ternary intermetallic compounds, HRE-TM-X (X = *p*-block elements) with the stoichiometric ratio of 1:1:2, have received extensive attention for their diverse crystal structure and unique magnetic properties [34–47]. Their magnetic phase transition and magnetocaloric properties can be varied depending on the TM and *p*-block elements. For TM = Ni and X = Al, the samples crystallize in the orthorhombic MgCuAl$_2$-type structure, presenting ferromagnetic (FM) order at low temperatures (Curie temperature (T_C) ranges around 2.4–28.0 K) [39–41]. For X = Si, the compounds crystallize in the CeNiSi$_2$-type structure, revealing antiferromagnetic order at low temperatures (Néel temperature ranges around 3.0–25.0 K) [44]. When X = Ga, depending on the RE element, two different types of crystal structures have been reported [46]: NdNiGa$_2$-type for RE = La–Nd, Sm or Gd and MgCuAl$_2$-type for RE = Y or Tb–Lu.

[1] Key Laboratory of Novel Materials for Sensor of Zhejiang Province & School of Electronics and Information Engineering, Hangzhou Dianzi University, Hangzhou 310012, China
[2] Departamento de Física de la Materia Condensada, ICMS-CSIC, Universidad de Sevilla, P.O. Box 1065. 41080-Sevilla, Spain
[3] State Key Laboratory of Advanced Special Steels & Shanghai Key Laboratory of Advanced Ferrometallurgy & School of Materials Science and Engineering, Shanghai University, Shanghai 200072, China
* Corresponding authors (emails: ykzhang@hdu.edu.cn (Zhang Y); jylaw@us.es (Law JY))

For the former structure, CeNiGa$_2$ and GdNiGa$_2$ were reported to show antiferromagnetic ordering at 4 and 22 K, respectively, and both direct and inverse MCE were observed in these two samples [48,49]. On the other hand, for MgCuAl$_2$-type gallides, although their MCE properties have not been reported, the isostructural aluminides exhibit excellent direct MCE in low temperature range, making it of interest to investigate the magnetocaloric behavior and properties of MgCuAl$_2$-type gallides. Hence, in this work, with the aim of obtaining suitable materials for cryogenic applications, we vary the type of HRE elements in the HRENiGa$_2$ system (HRE = Dy, Ho, or Er) and investigate their influence on the structural, thermomagnetic, and magnetocaloric behavior.

EXPERIMENTAL SECTION

A series of polycrystalline samples were fabricated by arc-melting from high-purity (at least 99.9%) elements in an Ar atmosphere with a nominal composition of HRENiGa$_2$ (HRE = Dy, Ho, or Er). An excess of 2 wt% of HRE elements was used to compensate for the losses caused by volatilization during the arc-melting process. The obtained ingots were wrapped in the Ta foil and sealed in a quartz tube for annealing. The annealing process was performed in a muffle furnace at 1073 K for one week, and then quenched in ice water. The phase and crystal structure analysis of the HRENiGa$_2$ was performed by X-ray diffraction (XRD) using a Bruker D8 diffractometer (Cu-Kα radiation). The magnetization data of the HRENiGa$_2$ were collected using the Vibrating Sample Magnetometer (VSM) option of the physical properties measurement system (PPMS-9).

RESULTS AND DISCUSSION

Fig. 1a displays the powder XRD as well as the Rietveld refinement results for DyNiGa$_2$, HoNiGa$_2$, and ErNiGa$_2$ compounds. Both DyNiGa$_2$ and HoNiGa$_2$ samples are single-phase crystallizing in the orthorhombic MgCuAl$_2$-type structure (*Cmcm* space group). While for ErNiGa$_2$, extra diffraction peaks corresponding to the Er$_2$O$_3$ phase (~1.0 wt%) are detected. The refined factors (included in Fig. 1a) reveal a good agreement between the structural model and the experimental data, being the weighted profile R factor (R_{wp}) of ~10% and a goodness of fit (GoF) of 1.5–1.9 [50]. The refined lattice parameters a and c are shown in Fig. 1b. It is worth noting that the lattice parameters decrease monotonically with the decrease of RE ion radius. A schematic of the crystal structure for HRENiGa$_2$ is included in Fig. 1c. HRE and Ni atoms occupy the same Wyckoff sites of 4c with the $m2m$ point symmetry, whereas Ga occupies the 8f sites with the $m..$ point symmetry.

The temperature dependence of magnetization (M) and reciprocal susceptibility ($1/\chi$) at $\mu_0 H = 1$ T for HRENiGa$_2$ are shown in Fig. 2a. From the M-T curves, all samples undergo a gradual magnetic transition from FM to paramagnetic (PM) states. The T_C can be estimated by the derivative of M-T curves (dM/dT-T curves) under the field of 0.01 T, which are also shown in Fig. 2b. The corresponding temperatures of the inflection points are 46.0, 26.0, and 11.0 K for DyNiGa$_2$, HoNiGa$_2$, and ErNiGa$_2$ compounds, respectively. According to the Ruderman-Kittel-Kasuya-Yosida (RKKY) indirect interaction theory [51], the T_C for RE-based compounds will be expected to be proportional to the de Gennes factor (dG). This factor is determined by the Lande factor (g) and the total orbital quantum number (J):

$$dG = (g-1)^2 J(J+1). \tag{1}$$

The relationship between T_C and dG for the samples is shown in the inset of Fig. 2b. As expected, a positive linear trend is observed, revealing the dominant role of RE-RE long-range interaction, which is consistent with previously reported data [46]. A linear trend is observed from the $1/\chi$-T curves (Fig. 2a), indicating that all the samples obey the Curie-Weiss law in the PM region:

$$1/\chi = \frac{1}{C}(T - \theta_P), \tag{2}$$

where θ_P is the PM Curie temperature and C is the Curie con-
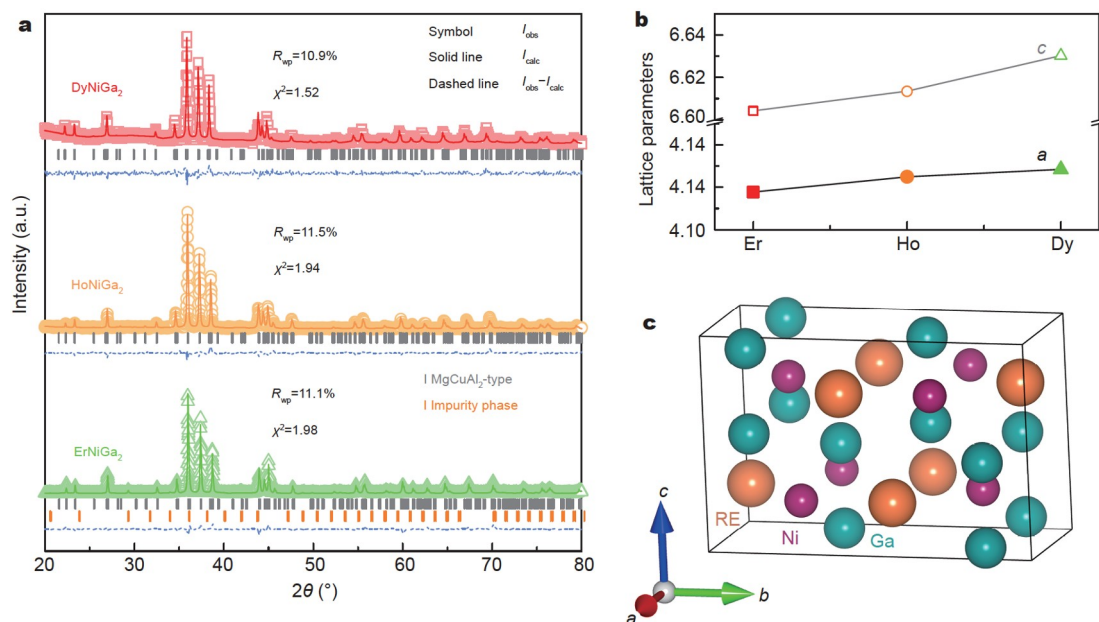
Figure 1 (a) Powder XRD patterns (room temperature) and the Rietveld refinement results for HRENiGa$_2$ compounds. (b) The lattice parameters as a function of RE elements. (c) Schematic of the MgCuAl$_2$-type crystal structure in these compounds.
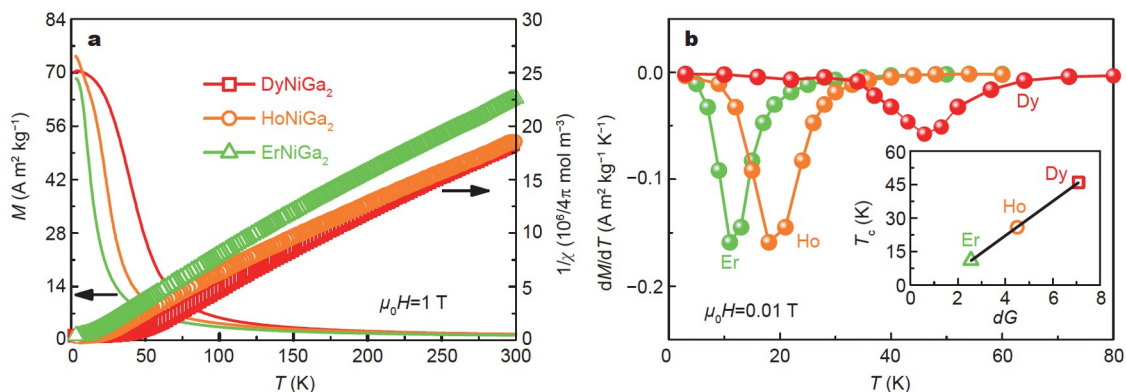
Figure 2 (a) The $M(T)$ and $1/\chi(T)$ curves under a magnetic field of 1 T for the HRENiGa$_2$ compounds. (b) dM/dT vs. T curves for the studied compounds. The inset displays the relation between T_C and dG factor.

stant which can be expressed by the following formula:

$$C = \frac{N_A \mu_{eff}^2 \mu_B^2}{3k_B},\tag{3}$$

where N_A is the Avogadro's number, k_B is the Boltzmann constant, μ_B is the Bohr magneton, and μ_{eff} is the effective magnetic moment. Therefore, according to the $1/\chi$-T curves, μ_{eff} and θ_P values can be estimated from the linear fit. The obtained values are 10.67 μ_B for DyNiGa$_2$, 10.62 μ_B for HoNiGa$_2$, and 9.61 μ_B for ErNiGa$_2$, which are very close to the values calculated by Hund's rules, i.e., 10.64 μ_B for Dy^{3+}, 10.60 μ_B for Ho^{3+}, and 9.58 μ_B for Er^{3+} [51]. This shows that the RE elements play a major magnetic contribution in these compounds. In addition, the θ_P is determined from the intercept of the fittings with the temperature axis, obtaining 29.3, 11.4, and 7.5 K for DyNiGa$_2$, HoNiGa$_2$, and ErNiGa$_2$, respectively. The positive values of θ_P prove the FM ground state in the studied series.

For exploring the magnetocaloric performance of these compounds, magnetization isotherms were measured at different temperatures around T_C (displayed in Fig. 3). It is observed that all samples show FM characteristic at low temperatures ($T < T_C$) whereas PM characteristic at high temperatures ($T > T_C$), in agreement with the previous M-T results. In addition, $M(H)$ loops measured for the three samples show negligible magnetic hysteresis (coercivity values of 30 mT for DyNiGa$_2$, 20 mT for HoNiGa$_2$ and 10 mT for ErNiGa$_2$). Using these isothermal magnetization curves, the isothermal entropy change (ΔS_{iso}) can be indirectly determined based on thermodynamic Maxwell relations from:

$$\Delta S_{iso}(T,H) = \mu_0 \int_0^H \left(\frac{\partial M(T,H)}{\partial T} \right)_H dH.\tag{4}$$

The calculated $|\Delta S_{iso}|$ values versus temperature for the studied compounds are plotted in Fig. 4a–c under several selected magnetic field changes (ΔH). For all the compounds, the values of $|\Delta S_{iso}|$ gradually increase as ΔH increases. For ΔH of 0–5 T, the maximum $|\Delta S_{iso}|$ values ($|\Delta S_{iso}^{max}|$) and their corresponding peak temperatures (T^{peak}) are found to be 6.2 J kg^{-1} K^{-1} and 41.5 K, 10.4 J kg^{-1} K^{-1} and 24.5 K, as well as 11.4 J kg^{-1} K^{-1} and 12.0 K for Dy-, Ho-, and Er-containing samples, respectively. It is highlighted that in the case of the Ho-containing compound, the magnetocaloric response is within the range of the H$_2$ liquefaction temperature (20.4 K). For the Er-containing sample, its T^{peak} shifts to higher temperatures gradually with increasing
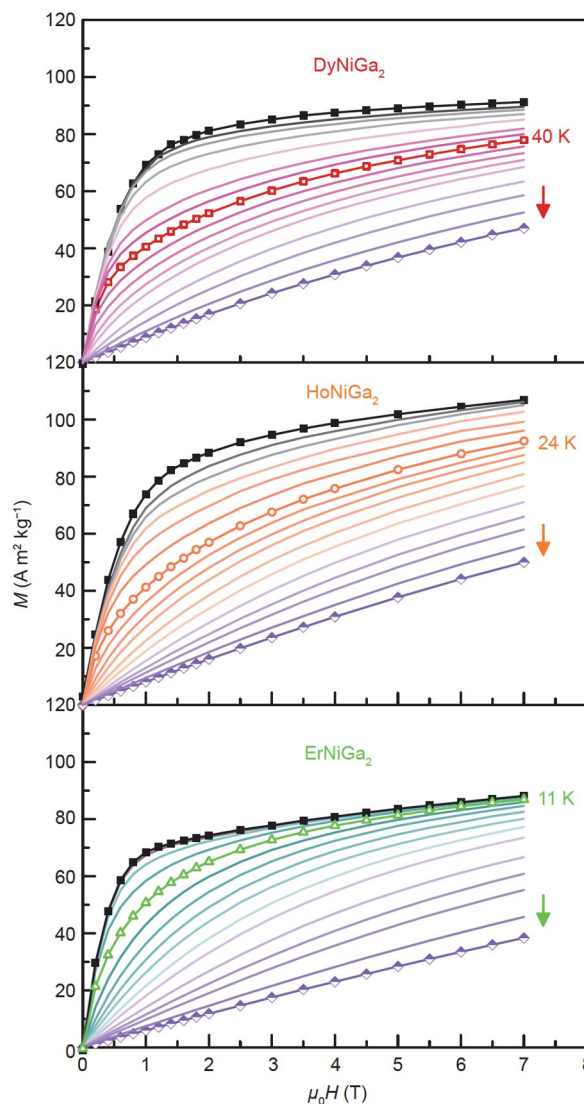
Figure 3 Magnetization isotherms measured around the transition temperatures (T_t) for the studied compounds. Arrows indicate the increase of temperature.

external field in contrast to DyNiGa$_2$ and HoNiGa$_2$ whose T^{peak} remains unaffected with fields. This can be ascribed to the
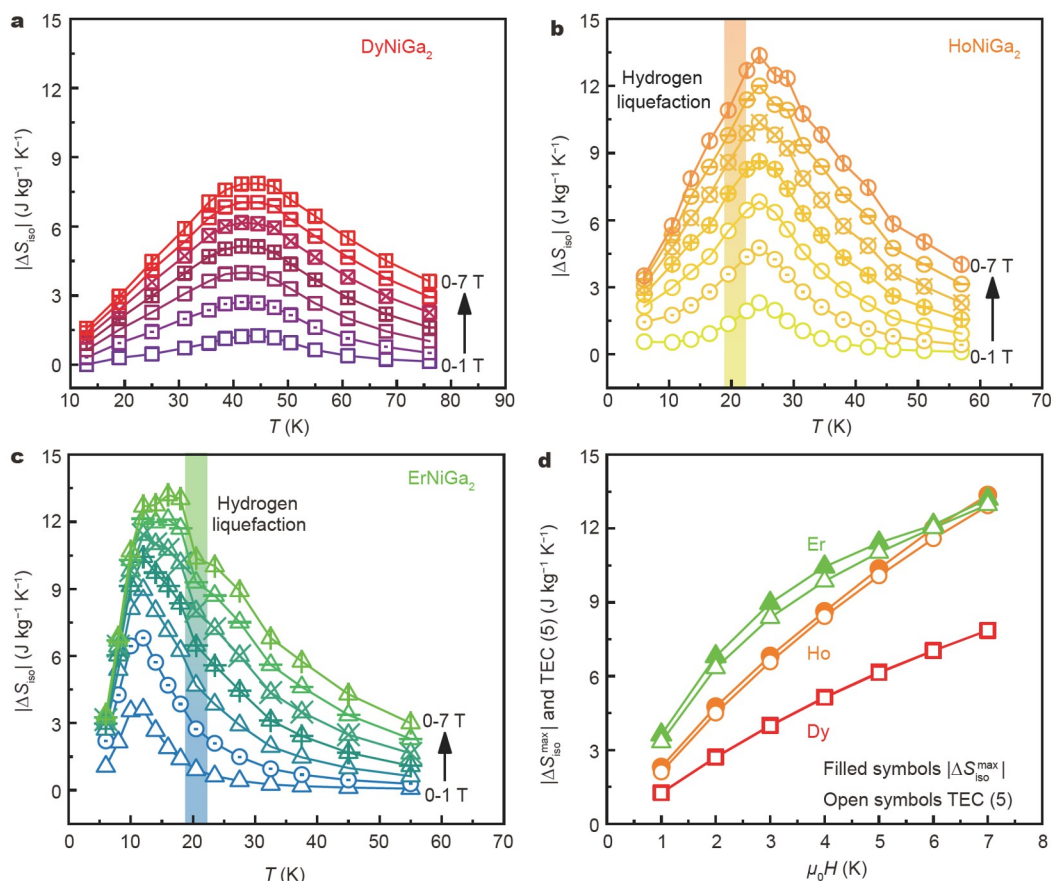
Figure 4 (a–c) The isothermal entropy change (ΔS_{iso}) *vs.* temperature curves for the studied compounds. (d) The field dependence of $|\Delta S_{iso}^{max}|$ and TEC(5) for the studied compounds.

critical exponents deviating from mean field for ErNiGa$_2$ [52]. When ΔH increases to 0–7 T, the T^{peak} value obtained for ErNiGa$_2$ is 18 K, which is close to the H$_2$ liquefaction temperature.

To quantify the cooling efficiency of the compounds, the relative cooling power (RCP) is calculated by the following equation:

$$\text{RCP} = -\Delta S_{iso}^{max} \times \delta T_{FWHM}, \tag{5}$$

where δT_{FWHM} is the full temperature width at a half maximum of the $|\Delta S_{iso}|$ peak. For 0–5 T, the RCP values are 275 J kg^{-1} for DyNiGa$_2$, 302 J kg^{-1} for HoNiGa$_2$, as well as 238 J kg^{-1} for ErNiGa$_2$, respectively. Additionally, the values of δT_{FWHM} are 44.6, 29.1, and 20.9 K for Dy-, Ho-, and Er-containing samples, respectively.

Griffith *et al.* [53] proposed the temperature-averaged magnetic entropy change (TEC) as another figure of merit to evaluate the magnetocaloric performance of the materials. For a given temperature span (ΔT_{lift}), the TEC(ΔT_{lift}) can be estimated using the following formula:

$$\text{TEC}(\Delta T_{lift}) = \frac{1}{\Delta T_{lift}} \max_{T_{mid}} \left\{ \int_{T_{mid} - \frac{\Delta T_{lift}}{2}}^{T_{mid} + \frac{\Delta T_{lift}}{2}} \Delta S_{iso}(T)\, dT \right\}, \tag{6}$$

where T_{mid} refers to the central temperature to make sure the TEC(ΔT_{lift}) achieves the maximum value. In this work, we chose ΔT_{lift} of 5 K and the TEC(5) values were determined to be 6.13, 10.07, and 11.03 J kg^{-1} K^{-1} for Dy, Ho and Er, which are 98.9%,

96.8%, and 96.7% of $|\Delta S_{iso}^{max}|$ values, respectively, as shown in Fig. 4d. This indicates that the compounds can properly operate as magnetic refrigerant (e.g., in active magnetic regenerator (AMR) cycles) with a working span of 5 K with performance close to their maximums.

It can be observed that while the maximum MC response of HoNiGa$_2$ compound is slightly above the H$_2$ liquefaction temperature, that of ErNiGa$_2$ is slightly below. Therefore, it is worth studying the existence of a composite material based on both HoNiGa$_2$ and ErNiGa$_2$, which would operate in a broad temperature range around the desired H$_2$ liquefaction temperature. Moreover, composites with two or more phases were found to be helpful in obtaining table-like MCE which is required for an ideal Ericsson cycle [27,54–57]. To explore this, we estimate the total values of $|\Delta S_{iso}|$ and TEC(ΔT_{lift} = 10, 15, and 20 K) under ΔH of 0–5 T for the xHoNiGa$_2$ + (1−x)ErNiGa$_2$ composite (where x is the mass fraction of the HoNiGa$_2$ compound in the composite, being $0 \leq x \leq 1$). This magnitude is selected as it is equivalent to the average value of magnetic entropy change over a wide temperature range (i.e., ΔT_{lift}), which is more representative for MCE performance evaluation. We found an optimal table-like MCE for $x = 0.5$ composite, having an isothermal entropy change of 8.7 J kg^{-1} K^{-1} with the temperature range of 11–25 K as presented in Fig. 5a, showing the potential of this composite for Ericsson cycle MR. Fig. 5b displays the $|\Delta S_{iso}^{max}|$ and TEC values as a function of the composite composition. It can be observed that the TEC values for 10, 15, and 20 K working span for $x = 0.5$ and 0.6 composites are much closer to
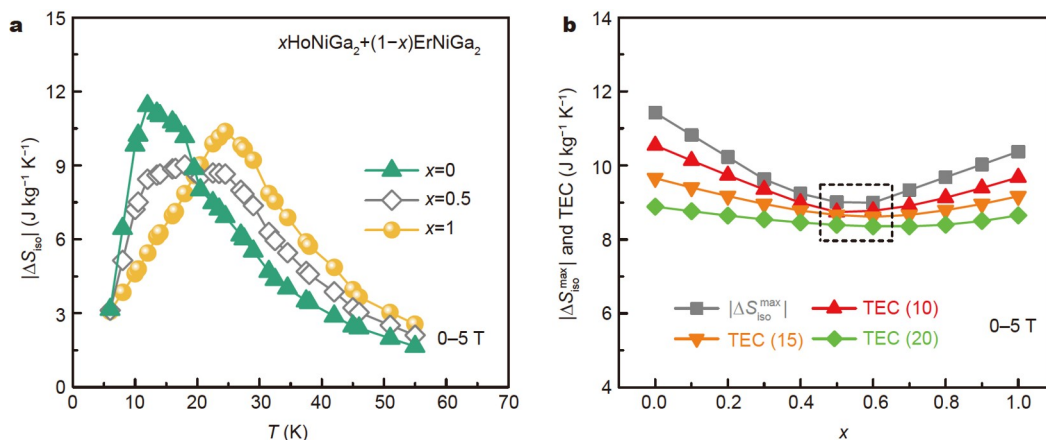
Figure 5 (a) $|\Delta S_{iso}|$ *vs.* T curves for the xHoNiGa$_2$ + (1−x)ErNiGa$_2$ composite for ΔH of 0–5 T. (b) The $|\Delta S_{iso}^{max}|$ and TEC (ΔT_{lift} = 10, 15, and 20 K) as a function of x (the mass fraction of HoNiGa$_2$) for the composite.
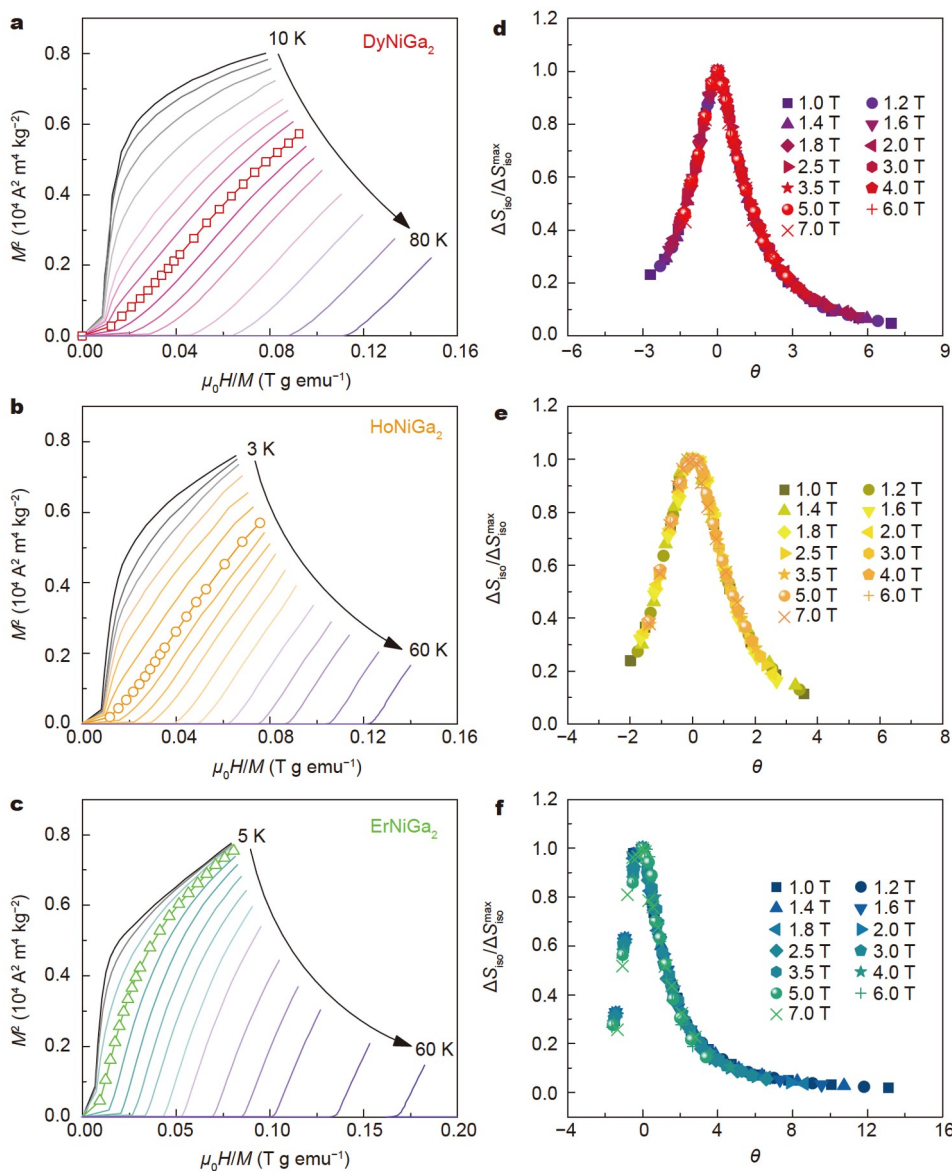
Figure 6 The Arrott plots (M^2 *versus* H/M) (a–c) and $\Delta S_{iso}(T)/\Delta S_{iso}^{max}$ *vs.* the rescaled temperature (θ) (d–f) for the studied compounds.
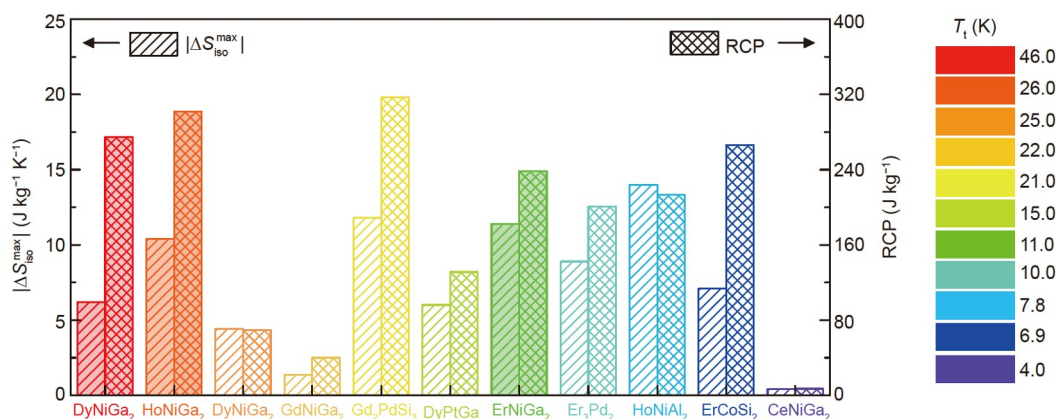
Figure 7 Magnetocaloric parameters ($|\Delta S_{iso}^{max}|$ and RCP) for the HRENiGa$_2$ compounds compared with other RETX$_2$ systems [34,41,44,48,49] and some recently reported cryogenic materials [59–61] for 0–5 T. The color legend on the right indicates the different T_t for each sample.

the $|\Delta S_{iso}^{max}|$ (highlighted by a dashed box), reinforcing the excellent table-like behavior (i.e., ΔS_{iso} is relatively constant and similar to $|\Delta S_{iso}^{max}|$ over the various ΔT_{lift} range values) and performance of those composites.

As MCE response is linked to the nature of magnetic transitions, it is thus important to determine the order of phase transitions for practical applications mainly to take into account the reversibility of the response. To confirm the nature of magnetic transitions, the Arrott plots (i.e., M^2 versus H/M curves) were constructed by applying the Banerjee's criterion [58] (Fig. 6a–c). It can be inferred that the three compounds undergo a second-order phase transition (SOPT) since all isotherms show positive slopes, according to the Banerjee's criterion.

In addition, Franco et al. [52] have introduced a criterion that a universal curve could be achieved for magnetocaloric materials undergoing SOPT upon rescaling the ΔS_{iso} vs. T curves for different ΔH. For the universal curve construction, the magnetic entropy change axis and temperature axis were changed to $\Delta S_{iso}(T)/\Delta S_{iso}^{max}$ and θ, respectively, where θ was defined independently below and above T_C as follows:

$$\theta = \begin{cases} -(T - T_C)/(T_{r1} - T_C) & \text{for } T \leqslant T_C, \\ (T - T_C)/(T_{r2} - T_C) & \text{for } T > T_C, \end{cases} \quad (7)$$

where T_{r1} and T_{r2} ($T_{r1} < T_C < T_{r2}$) denote two reference temperatures and their corresponding $\Delta S_{iso}(T_{r1})/\Delta S_{iso}^{max} = \Delta S_{iso}(T_{r2})/\Delta S_{iso}^{max} = 0.6$. Fig. 6d–f present the normalized $\Delta S_{iso}(T)/\Delta S_{iso}^{max}$ vs. θ curves for the DyNiGa$_2$, HoNiGa$_2$, and ErNiGa$_2$ compounds, respectively. It can be observed that all rescaled curves are unaffected by the magnetic field and collapse onto a universal curve, revealing the SOPT nature for the three studied samples. These results are in excellent agreement to those of the Banerjee's criterion.

Fig. 7 displays the $|\Delta S_{iso}^{max}|$ and RCP values of the studied samples and their T_t indicated by the color legend. For comparison, other RETMX$_2$ systems and some recently reported cryogenic materials falling in the range of the H$_2$ liquefaction temperature have been included. It can be seen that the magnetocaloric parameters of our studied MgCuAl$_2$-type gallides are much larger than those of the NdNiGa$_2$-type ones, which can be attributed to the favored FM ground state. In addition, the present samples also show competitive cooling efficiency compared with the isostructural MgCuAl$_2$-type aluminides, CeNiSi$_2$-type silicides, and some other materials, making them potential candidates for cryogenic applications.

CONCLUSIONS

HRENiGa$_2$ series (with HRE = Dy, Ho, and Er) crystallizing in the MgCuAl$_2$-type crystal structure were successfully synthesized by arc melting. Rietveld refinement results show that all the samples are almost single-phase (99 wt% of the main phase). All three compounds undergo an FM-PM magnetic phase transition at low temperatures, around 46.0, 26.0, and 11.0 K for Dy-, Ho-, and Er-containing samples, respectively. The second order nature of the magnetic phase transitions was verified by the Banerjee's criterion and magnetocaloric universal curve method. Regarding the magnetocaloric response, the maximum $|\Delta S_{iso}|$ values for 0–5 T are 6.2, 10.4, and 11.4 J kg^{-1} K^{-1} for Dy, Ho, and Er, respectively. The temperature span of these responses, quantified by δT_{FWHM} values, are 44.6 K for DyNiGa$_2$, 29.1 K for HoNiGa$_2$, and 20.9 K for ErNiGa$_2$, showing good cooling performance in a broad temperature range. This has also been checked by the TEC(5) parameter, which shows values rather close to their maximum capabilities (around 99%–97%). For HoNiGa$_2$ and ErNiGa$_2$ compounds, their peak temperatures of maximum isothermal entropy changes are close to the H$_2$ liquefaction temperature, making them of great value for magnetocaloric liquefaction systems. Moreover, we illustrate the excellent magnetocaloric performance of a hypothetical HoNiGa$_2$ and ErNiGa$_2$ composite which would exhibit a notable table-like MCE in a broad temperature range around the desired H$_2$ liquefaction temperature (8.7 J kg^{-1} K^{-1} around 11–25 K).

1   Shen BG, Sun JR, Hu FX, et al. Recent progress in exploring magnetocaloric materials. Adv Mater, 2009, 21: 4545–4564

2   Franco V, Blázquez JS, Ipus JJ, et al. Magnetocaloric effect: From materials research to refrigeration devices. Prog Mater Sci, 2018, 93: 112–232

3   Tegus O, Brück E, Buschow KHJ, et al. Transition-metal-based magnetic refrigerants for room-temperature applications. Nature, 2002, 415: 150–152

4   Zhang YK. Review of the structural, magnetic and magnetocaloric properties in ternary rare earth RE_2T_2X type intermetallic compounds. J

Alloys Compd, 2019, 787: 1173–1186

5   Law JY, Moreno-Ramírez LM, Blázquez JS, *et al*. Gd+GdZn biphasic magnetic composites synthesized in a single preparation step: Increasing refrigerant capacity without decreasing magnetic entropy change. J Alloys Compd, 2016, 675: 244–247

6   Li J, Law JY, Huo J, *et al*. Magnetocaloric effect of Fe-RE-B-Nb (RE = Tb, Ho or Tm) bulk metallic glasses with high glass-forming ability. J Alloys Compd, 2015, 644: 346–349

7   Law JY, Franco V. Pushing the limits of magnetocaloric high-entropy alloys. APL Mater, 2021, 9: 080702

8   Yin H, Law JY, Huang Y, *et al*. Enhancing the magnetocaloric response of high-entropy metallic-glass by microstructural control. Sci China Mater, 2022, 65: 1134–1142

9   Law JY, Díaz-García Á, Moreno-Ramírez LM, *et al*. Increased magnetocaloric response of FeMnNiGeSi high-entropy alloys. Acta Mater, 2021, 212: 116931

10 Law JY, Moreno-Ramírez LM, Díaz-García Á, *et al*. MnFeNiGeSi high-entropy alloy with large magnetocaloric effect. J Alloys Compd, 2021, 855: 157424

11 Zhang Y, Zhu J, Li S, *et al*. Achievement of giant cryogenic refrigerant capacity in quinary rare-earths based high-entropy amorphous alloy. J Mater Sci Tech, 2022, 102: 66–71

12 Ma Z, Dong X, Zhang Z, *et al*. Achievement of promising cryogenic magnetocaloric performances in La$_{1-x}$Pr$_x$Fe$_{12}$B$_6$ compounds. J Mater Sci Tech, 2021, 92: 138–142

13 Law JY, Díaz-García Á, Moreno-Ramírez LM, *et al*. How concurrent thermomagnetic transitions can affect magnetocaloric effect: The Ni$_{49+x}$Mn$_{36-x}$In$_{15}$ Heusler alloy case. Acta Mater, 2019, 166: 459–465

14 Law JY, Franco V, Conde A, *et al*. Modification of the order of the magnetic phase transition in cobaltites without changing their crystal space group. J Alloys Compd, 2019, 777: 1080–1086

15 Zhang Y, Zhu J, Li S, *et al*. Magnetic properties and promising magnetocaloric performances in the antiferromagnetic GdFe$_2$Si$_2$ compound. Sci China Mater, 2022, 65: 1345–1352

16 Li Y, Qin L, Huang S, *et al*. Enhanced magnetocaloric performances and tunable martensitic transformation in Ni$_{35}$Co$_{15}$Mn$_{35-x}$Fe$_x$Ti$_{15}$ all-d-metal Heusler alloys by chemical and physical pressures. Sci China Mater, 2022, 65: 486–493

17 Li L, Yan M. Recent progress in the magnetic and cryogenic magnetocaloric properties of *RE*$_2$*TMTM′*O$_6$ double perovskite oxides. J Mater Sci Tech, 2022, :

18 Li L, Yan M. Recent progresses in exploring the rare earth based intermetallic compounds for cryogenic magnetic refrigeration. J Alloys Compd, 2020, 823: 153810

19 Numazawa T, Kamiya K, Utaki T, *et al*. Magnetic refrigerator for hydrogen liquefaction. Cryogenics, 2014, 62: 185–192

20 Zhang Y, Wu B, Guo D, *et al*. Magnetic properties and promising cryogenic magneto-caloric performances of Gd$_{20}$Ho$_{20}$Tm$_{20}$Cu$_{20}$Ni$_{20}$ amorphous ribbons. Chin Phys B, 2021, 30: 017501

21 Wang Y, Guo D, Wu B, *et al*. Magnetocaloric effect and refrigeration performance in *RE*$_{60}$Co$_{20}$Ni$_{20}$ (RE = Ho and Er) amorphous ribbons. J Magn Magn Mater, 2020, 498: 166179

22 Wu B, Zhang Y, Guo D, *et al*. Structure, magnetic properties and cryogenic magneto-caloric effect (MCE) in *RE*$_2$FeAlO$_6$ (*RE* = Gd, Dy, Ho) oxides. Ceram Int, 2021, 47: 6290–6297

23 Li L, Xu P, Ye S, *et al*. Magnetic properties and excellent cryogenic magnetocaloric performances in B-site ordered *RE*$_2$ZnMnO$_6$ (RE = Gd, Dy and Ho) perovskites. Acta Mater, 2020, 194: 354–365

24 Zhang Y, Tian Y, Zhang Z, *et al*. Magnetic properties and giant cryogenic magnetocaloric effect in B-site ordered antiferromagnetic Gd$_2$MgTiO$_6$ double perovskite oxide. Acta Mater, 2022, 226: 117669

25 Xu P, Ma Z, Wang P, *et al*. Excellent cryogenic magnetocaloric performances in ferromagnetic Sr$_2$GdNbO$_6$ double perovskite compound. Mater Today Phys, 2021, 20: 100470

26 Franco V, Blázquez JS, Ingale B, *et al*. The magnetocaloric effect and magnetic refrigeration near room temperature: Materials and models. Annu Rev Mater Res, 2012, 42: 305–342

27 Guo D, Moreno-Ramírez LM, Romero-Muñiz C, *et al*. First- and second-order phase transitions in *RE*$_6$Co$_2$Ga (*RE* = Ho, Dy or Gd) cryo-

genic magnetocaloric materials. Sci China Mater, 2021, 64: 2846–2857

28 Castro PB, Terashima K, Yamamoto TD, *et al*. Machine-learning-guided discovery of the gigantic magnetocaloric effect in HoB$_2$ near the hydrogen liquefaction temperature. NPG Asia Mater, 2020, 12: 35

29 Luo Q, Zhao DQ, Pan MX, *et al*. Magnetocaloric effect of Ho-, Dy-, and Er-based bulk metallic glasses in helium and hydrogen liquefaction temperature range. Appl Phys Lett, 2007, 90: 211903

30 Palacios E, Tomasi C, Sáez-Puche R, *et al*. Effect of Gd polarization on the large magnetocaloric effect of GdCrO$_4$ in a broad temperature range. Phys Rev B, 2016, 93: 064420

31 Shinde KP, Jang SH, Kim JW, *et al*. Magnetocaloric properties of TbN, DyN and HoN nanopowders prepared by the plasma arc discharge method. Dalton Trans, 2015, 44: 20386–20391

32 Zhang H, Shen BG, Xu ZY, *et al*. Large reversible magnetocaloric effects in ErFeSi compound under low magnetic field change around liquid hydrogen temperature. Appl Phys Lett, 2013, 102: 092401

33 Terada N, Mamiya H. High-efficiency magnetic refrigeration using holmium. Nat Commun, 2021, 12: 1212

34 Guo D, Zhang Y, Wu B, *et al*. Structural, magnetic properties and magneto-caloric performances in the antiferromagnetic RECoSi$_2$ (RE = Er and Tm) compounds. J Alloys Compd, 2020, 843: 156016

35 Pelizzone M, Braun HF, Muller J. Magnetic properties of RCoSi$_2$ compounds (R = rare earth). J Magn Magn Mater, 1982, 30: 33–36

36 Penc B, Szytuła A, Wawrzyńska E, *et al*. Magnetic structures and magnetic phase transitions in TbCoSi$_2$. J Alloys Compd, 2004, 366: 120–123

37 Radzieowski M, Stegemann F, Bönnighausen J, *et al*. Physical and magnetocaloric properties of TbPdAl$_2$ and the ferromagnetic solid solution Tb$_{1-x}$Lu$_x$PdAl$_2$ (x = 0.1–0.9). Inorg Chem, 2020, 59: 1137–1144

38 Wu X, He W, Yang T, *et al*. The magnetic and electronic properties of REAgSb$_2$ compounds. J Magn Magn Mater, 2021, 519: 167442

39 Dembele SN, Ma Z, Shang YF, *et al*. Large magnetocaloric effect of GdNiAl$_2$ compound. J Magn Magn Mater, 2015, 391: 191–194

40 Xu JW, Zheng XQ, Yang SX, *et al*. Low working temperature near liquid helium boiling point of RNiAl$_2$ (R = Tm, Tb and Gd) compounds with large magnetocaloric effect. J Appl Phys, 2019, 125: 225102

41 Zhang Y, Guo D, Yang Y, *et al*. Magnetic properties and magnetocaloric effect in the aluminide RE NiAl$_2$ (RE = Ho and Er) compounds. Intermetallics, 2017, 88: 61–64

42 Li R, Ma Z, Balfour EA, *et al*. Critical behavior study in GdNiAl$_2$ intermetallic compound. J Alloys Compd, 2016, 658: 672–677

43 Radzieowski M, Stegemann F, Doerenkamp C, *et al*. Correlations of crystal and electronic structure *via* NMR and X-ray photoelectron spectroscopies in the RETMAl$_2$ (RE = Sc, Y, La-Nd, Sm, Gd-Tm, Lu; TM = Ni, Pd, Pt) series. Inorg Chem, 2019, 58: 7010–7025

44 Zhang B, Zheng XQ, Zhang Y, *et al*. Magnetic properties and magnetocaloric effects of RNiSi$_2$ (R = Gd, Dy, Ho, Er, Tm) compounds. AIP Adv, 2018, 8: 056423

45 Grin Y, Hiebl K, Rogl P, *et al*. Crystal structure and magnetic behaviour of ternary YbTGa$_2$ compounds (T = Ni, Pd, Pt) and quaternary solid solutions YbPd$_{1-x}$Ag$_x$Ga$_2$. J Alloys Compd, 1996, 239: 127–130

46 Romaka VA, Grin YN, Yarmolyuk YP, *et al*. Magnetic and crystallographic characteristics of RNiGa$_2$ compounds (R = rare-earth metal). Ukr Fiz Zh, 1983, 28: 227–230

47 Vasylechko L, Burkhardt U, Schnelle W, *et al*. Order/disorder in YbNi$_{1+x}$Ga$_{2+x}$ (x ≤ 0.08): Crystal structure, thermal expansion and magnetic properties. Solid State Sci, 2012, 14: 746–760

48 Yao J, Garshev AV, Knotko AV, *et al*. The Ce-Ni-Ga system at 670/870 K: Magnetic properties and heat capacity of ternary compounds. J Solid State Chem, 2021, 294: 121895

49 Chen T, Yao J, Knotko AV, *et al*. The Gd-Ni-Ga system at 870 K as a representative of rare-earth nickel gallides: Crystal structure and magnetic properties. J Solid State Chem, 2022, 305: 122692

50 Toby BH. *R* factors in Rietveld analysis: How good is good enough? Powder Diffr, 2006, 21: 67–70

51 Legvold S. Chapter 3 Rare earth metals and alloys. Handb Ferromagn Mater, 1980, 1: 183–295

52 Franco V, Conde A. Scaling laws for the magnetocaloric effect in second order phase transitions: From physics to applications for the

characterization of materials. Int J Refrig, 2010, 33: 465–473

53 Griffith LD, Mudryk Y, Slaughter J, et al. Material-based figure of merit for caloric materials. J Appl Phys, 2018, 123: 034902

54 Li L, Kadonaga M, Huo D, et al. Low field giant magnetocaloric effect in RNiBC (R = Er and Gd) and enhanced refrigerant capacity in its composite materials. Appl Phys Lett, 2012, 101: 122401

55 Álvarez P, Sánchez Llamazares JL, Gorria P, et al. Enhanced refrigerant capacity and magnetic entropy flattening using a two-amorphous FeZrB(Cu) composite. Appl Phys Lett, 2011, 99: 232501

56 Law JY, Franco V. Magnetocaloric composite materials. In: Brabazon D (ed.). Encyclopedia of Materials: Composites. Amsterdam: Elsevier, 2021. 461–472

57 Zhang Y, Yang Y, Xu X, et al. Excellent magnetocaloric properties in RE_2Cu_2Cd (RE = Dy and Tm) compounds and its composite materials. Sci Rep, 2016, 6: 34192

58 Banerjee BK. On a generalised approach to first and second order magnetic transitions. Phys Lett, 1964, 12: 16–17

59 Mo ZJ, Shen J, Gao XQ, et al. Magnetic properties and magnetocaloric effect in the R_2PdSi_3 (R = Gd, Dy and Er) compounds. J Alloys Compd, 2015, 626: 145–149

60 Maji B, Ray MK, Modak M, et al. Magnetic properties and large reversible magnetocaloric effect in Er_3Pd_2. J Magn Magn Mater, 2018, 456: 236–240

61 França ELT, dos Santos AO, Coelho AA, et al. Magnetocaloric effect of the ternary Dy, Ho and Er platinum gallides. J Magn Magn Mater, 2016, 401: 1088–1092

Author contributions Zhang Y and Law JY designed the idea of the research. Guo D and Zhang Y performed the experiments. Guo D, Moreno-Ramírez LM, and Law JY performed the data analysis and prepared the manuscript. All the authors contributed to the general discussion and review and editing. Franco V and Zhang Y contributed to the conceptualization and supervision.

Conflict of interest The authors declare that they have no conflict of interest.

Dan Guo is a PhD student at the School of Materials Science and Engineering, Shanghai University (SHU), China. She is now a visiting scholar at the University of Seville, Spain, sponsored by the China Scholarship Council. Her research interests focus on magnetic properties and magnetocaloric effect of heavy rare-earth based compounds.

Jia-Yan Law obtained her PhD degree from the School of Materials Science and Engineering, Nanyang Technological University, Singapore. Currently, she is a postdoctoral researcher at the University of Seville (Spain), leading the research line "Functional High-Entropy Alloys". Her research interests include the development of magnetic and magnetocaloric materials, device and novel evaluation techniques as well as additive manufacturing.

Yikun Zhang received her PhD degree from Northeastern University (China); afterward, she was granted by the Alexander von Humboldt (AvH) scholarship for postdoctoral research. Currently, she is a professor at Hangzhou Dianzi University (China). Her research mainly focuses on designing and exploring magnetic functional materials, especially rare-earth-based magnetic refrigeration materials.

重稀土HRENiGa$_2$ (HRE = Dy, Ho或Er)化合物的优异低温磁热性能

郭丹[1,2,3], Luis M. Moreno-Ramírez[2], Jia-Yan Law[2*], 张义坤[1,3*], Victorino Franco[2]

摘要 RENiX$_2$化合物(其中RE为稀土元素，X为p区元素)在低温磁制冷应用中受到高度关注．它们根据元素的不同可以结晶成CeNiSi$_2$型、NdNiGa$_2$型或MgCuAl$_2$型晶体结构，并表现出不同类型的磁有序性从而影响其磁性．MgCuAl$_2$型铝化物由于具有有利的铁磁基态从而表现出比CeNiSi$_2$型硅化物和NdNiGa$_2$型镓化物更大的磁热性能．此外，RENiGa$_2$镓化物根据RE元素的不同可以结晶成NdNiGa$_2$或MgCuAl$_2$型结构．本文中，我们选择重稀土(HRE)元素来探索HRENiGa$_2$ (HRE = Dy, Ho或Er)镓化物的微观结构、磁有序和磁热性能．三种化合物均以MgCuAl$_2$型晶体结构结晶，并且随着温度的升高经历了从铁磁到顺磁的二级磁相转变．DyNiGa$_2$, HoNiGa$_2$和ErNiGa$_2$化合物的最大等温磁熵变($|\Delta S_{iso}^{max}|$)值分别为6.2, 10.4和11.4 J kg^{-1} K^{-1} (0–5 T)，这与许多最近报道的低温磁制冷材料性能相当．特别地，HoNiGa$_2$和ErNiGa$_2$化合物(包括它们的复合材料)在氢气液化的温度范围内表现出优异的磁热性能．